ACS APPLIED MATERIALS & INTERFACES

Research Article

www.acsami.org

Effects of Bis(imidazolium) Molten Salts with Different Substituents of Imidazolium Cations on the Performance of Efficient Dye-Sensitized Solar Cells

Sihang Bai, Chenghao Bu, Qidong Tai, Liangliang Liang, Yumin Liu, Sujian You, Zhenhua Yu, Shishang Guo,* and Xingzhong Zhao*

School of Physics and Technology, Key Laboratory of Artificial Micro/Nano Structures of Ministry of Education, Wuhan University, Wuhan, 430072, China

ABSTRACT: Bis(imidazolium) iodides (bis-Im$^+$I$^-$s) are synthesized with different substituents and used as electrolytes in dye-sensitized solar cells (DSSCs). Three kinds of low-volatility electrolytes are prepared by using 1,1′-methylene bis(3-imidazolium) diiodide (MIDI), 1,1′-methylene bis(3-*n*-methylimidazolium) diiodide (MMIDI), and 1,1′-methylene-bis(3-*n*-ethylimidazolium) diiodide (MEIDI) as the iodide sources. The effects of these substituents on the photovoltaic performance of the cells are investigated. It is found that the device shows a lower short-circuit photocurrent (J_{sc}), higher open-voltage (V_{oc}) and fill factor (*FF*) with the increased cation size in electrolyte. These results are explained by electrostatic interactions between the solvated Im$^+$ and the negatively charged species. Meanwhile, the explanation is supported by electrochemical impedance spectroscopy (EIS), cyclic voltammetry (CV), open circuit voltage decay (OCVD), and dark current measurements.

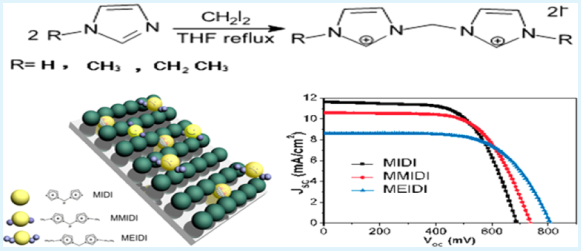

KEYWORDS: *triiodide/iodide redox couple, bis(imidazolium) iodide, low-volatility electrolyte, electrostatic interaction, dye-sensitized solar cells*

INTRODUCTION

Dye-sensitized solar cells (DSSCs) have drawn great attention over the past two decades as a promising energy source,[1−3] due to the potential for low-cost and efficient solar energy conversion.[4] Typical DSSCs consist of nanocrystalline titanium oxide (TiO_2) mesoporous film,[5,6] sensitizing dyes,[7,8] electrolytes[9−11] containing redox couple, and platinum-coated counter electrodes.[9,12,13] The electrolyte, as a critical component of DSSCs, plays an important role for completing the internal electrochemical circuit of a device by transferring electrons to the oxidized dye molecules. The liquid triiodide/iodide redox electrolyte has shown ideal kinetic properties of the rapid regeneration of the dye by I$^-$ and the slow recombination of I_3^- with photoinjected electrons in the TiO_2. As an important part of the state-of-the-art processing and technology, the liquid triiodide/iodide redox electrolytes have been investigated over past two decades, achieving efficiencies exceeding 11%.[14,15]

Lithium iodide (LiI) has a chief position in iodide sources of I_3^-/I$^-$ redox couple owing to its superior performance among varieties of iodide salts tested. However, the device based on LiI shows lower photovoltages and shorter electron lifetimes.[16] In addition, the properties of highly hygroscopic, air-sensitive and high cost of LiI restrict its commercial application in DSSCs. Recently, several types of iodides have been investigated as alternatives to LiI.[17−19] Imidazolium iodides have been used as both iodide sources[20,21] and additives[22,23] in DSSCs. However, bis(imidazolium) molten salts have not been applied to DSSCs as individual iodide sources and the impact of different substituents of bis(imidazolium) cations on the electrochemical behaviors of the I_3^-/I$^-$ electrolyte has never been investigated. As we know, bulkier cations lead to longer electron lifetimes and higher photovoltages for the better blocking of TiO_2 surface.[24] It is essential to improve the electrolyte via synthesizing a larger cation instead of Li$^+$ in the practical application of DSSCs.

Herein, we report the application of bis-Im$^+$I$^-$s with different substituents in size as individual iodide sources in DSSCs for the first time. The main difference in three kinds of bis-Im$^+$I$^-$s was the size of the substituent. Employing the electrolyte based on bis-Im$^+$I$^-$s with larger size of substituents, DSSC device shows a lower short-circuit photocurrent (J_{sc}), higher open-voltage (V_{oc}) and fill factor (*FF*). The mechanism of effect shown by different substituents was studied in our work. The results are discussed by cyclic voltammetry, *J-V* characteristics, electrochemical impedance spectroscopy (EIS), and open-circuit voltage decay (OCVD) test, enabling us to identify the underlying effect of bis-Im$^+$I$^-$s with different substituents on the performances of DSSCs.

Received: January 31, 2013
Accepted: April 1, 2013
Published: April 1, 2013

EXPERIMENTAL SECTION

Synthesis and Characterization of Bis(imidazolium) Iodides. The bis(imidazolium) iodides were synthesized according to Figure 1.[25] Detailed procedures are described below.

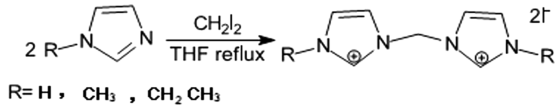

Figure 1. Synthesis route of 1,1′-methylene bis(3-imidazolium) diiodide (MIDI), 1,1′-methylene bis(3-*n*-methylimidazolium) diiodide (MMIDI), and 1,1′-methylene bis(3-*n*-ethylimidazolium) diiodide (MEIDI).

Preparation of 1,1′-Methylene Bis(3-imidazolium) Diiodide (MIDI). CH_2I_2 (13.39 g, 50 mmol) was added to tetrahydrofuran (THF) (60 mL) solution containing imidazole (4.08 g, 60 mmol). The solution was stirred at reflux temperature for 48 h then cooled and filtered to obtain a white powder. ^{1}HNMR (400 MHz, D_2O, ppm): δ 8.059 (s, 2H, NCHN), δ 7.053 (s, 2H, NCHC), δ 6.848 (s, 2H, NCHC), δ 6.066 (s, 2H, NCH_2N).

Preparation of 1,1′-Methylene Bis(3-n-methylimidazolium) Diiodide (MMIDI). CH_2I_2 (14.73 g, 55 mmol) was added to THF (120 mL) solution containing *n*-methylimidazolium (8.21 g, 100 mmol). The solution was refluxed while stirring magnetically for 72 h. The reaction mixture was allowed to cool and was filtered. The solution was heated and refluxed while stirring magnetically for 72 h. The reaction mixture was washed a few more times with THF and acetonitrile and filtered to gain a white powder. ^{1}HNMR (400 MHz, D_2O, ppm) of MIDI: δ 9.17 (s, 2H, NCHN), δ 7.72 (s, 2H, NCHC), δ 7.49 (s, 2H, NCHC), δ 6.62 (s, 2H, NCH_2N), δ 3.86 (s, 6H, CH_3).

Preparation of 1,1′-Methylene Bis(3-n-ethylimidazolium) Diiodide (MEIDI). A mixture of 14.73 g of CH_2I_2 (55 mmol), 120 mL of THF, and 9.61 g of *n*-ethylimidazole (100 mmol) was heated to 65 °C for 72 h. After cooling to room temperature, the white powder was washed a few more times with THF and acetonitrile. ^{1}HNMR (400 MHz, D_2O, ppm): δ 7.037 (s, 2H, NCHN), δ 6.944 (s, 2H, NCHC), δ 6.793 (s, 2H, NCHC), δ 5.970 (s, 2H, NCH2N), δ 2.587 (s, 4H, CH_2) δ 1.132 (s, 6H, CH_3)

Preparation of Electrolytes. The electrolytes were prepared by dissolving the bis-Im^+I^-s (cannot dissolve in other solvents) and I_2 into the mixture of DMSO and PC (vol:vol = 3:2). Solutions of 10 mM bis-Im^+I^-s, 1 mM I_2, and 0.1 M TBAT were used for CV measurements. The molar ratios of bis-Im^+I^-s and I_2 were optimized at 10 for MMIDI and 20 for MIDI and MEIDI in electrolytes used for DSSCs, and the concentrations of bis-Im^+I^-s were fixed at 0.25 M for all cases, besides 0.3 M TBP and 0.1 M TBAT were used as additives. The same electrolytes were also used for the tests in dummy cells.

Fabrication of DSSCs. TiO_2 photoelectrodes were prepared according to the previously reported method.[26] The solar cells were assembled by placing a platinum-sputtered FTO (counter electrode) on the N719 dye-sensitized photoelectrode. Dummy solar cells were assembled by placing a platinum-sputtered FTO with hot-melt Surlyn film (25 μm thickness, Geao Tech) as a spacer. The electrolyte was injected into the cell.

Characterization of DSSCs. Photovoltaic measurements were performed by applying external potential bias to the device under AM1.5 simulated illumination (Newport, 91192) with a power density of 100 $mW{\cdot}cm^{-2}$. The irradiated area of each cell was kept at 0.25 cm^2 by using a light-tight metal mask. Cyclic voltammetry was also performed on a CHI 660C (Shang Hai, China) electrochemical workstation with platinized FTO as working electrode, a Pt as auxiliary electrode, and an Ag/Ag^+ electrode as reference electrode at a 50 mVs^{-1} scan rate. Electrochemical impedance spectroscopy (EIS) measurements were performed by an electrochemical workstation (CHI660C, CH Instruments) with the frequency ranging from 100 kHz to 0.1 Hz in the illumination. EIS measurements of dummy cells were obtained in the frequency range from 100K Hz to 0.01 Hz at 0 V bias. For comparison, the similar pieces of photoelectrode were used for all kinds of electrolytes.

RESULTS AND DISCUSSION

Cyclic voltammetry (CV) was used to investigate the catalytic activity of electrode toward the I^-/I_3^- redox couple. MIDI, MMIDI, and MEIDI-based electrolytes were studied by CV employing Pt as working electrodes (Figure 2). Two

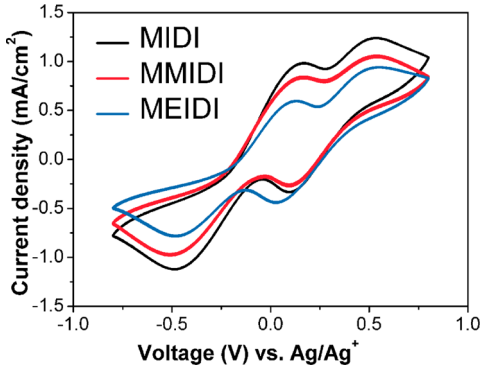

Figure 2. Cyclic voltammograms of MIDI electrolyte (10 mM MIDI, 1 mM I_2, 0.1 M TBAT, in DMSO and PC, vol:vol = 3:2), MMIDI electrolyte (10 mM MMIDI, 1 mM I_2, 0.1 M TBAT, in DMSO and PC, vol:vol = 3:2), and MEIDI electrolyte (10 mM MEIDI, 1 mM I_2, 0.1 M TBAT, in DMSO and PC, vol:vol = 3:2) obtained at a 50 mVs^{-1} scan rate. Reference electrode: Ag/Ag^+ reference electrode in acetonitrile.

representative pairs of redox waves of I^-/I_3^- were observed for all electrolytes, which showed similar redox behaviors. As we all know, the left and the right pairs are explained to be the oxidation and reduction of I^-/I_3^- and I_3^-/I_2,[27] respectively. The characteristics of the left pair of peaks reflected the apparent catalytic activity of the counter electrodes for electrolyte.[26,28] In comparison with that of the electrolyte based on MMIDI and MEIDI, the higher reduction peak current density of the MIDI-based electrolyte suggests superior apparent catalytic activity, which means electrolytes based on MIDI have the best apparent catalytic activity on counter electrodes at the same molar ratio.

The MMIDI/I_2 molar ratio in the new electrolyte was preliminarily optimized and fixed at 10, which means a 20 I^-/I_2 molar ratio in our previous work (unpublished), similar electrolyte based on MIDI and MMIDI for iodide source was also optimized. Figure 3 shows the variation of photovoltaic

dx.doi.org/10.1021/am400337d | ACS Appl. Mater. Interfaces 2013, 5, 3356−3361

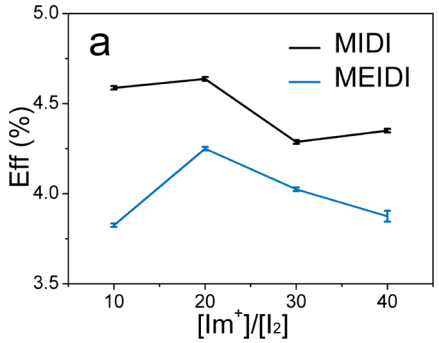

Figure 3. Optimization of molar ratio of MIDI/I_2 and MEIDI/I_2-based electrolytes.

parameters with Im^+I^-/I_2 molar ratio for the cell. It is found that the conversion efficiency of DSSC increases slightly from 10 to 20 molar ratio, then decreases after 20 I^-/I_2 molar ratio. Taking into account the best conversion efficiency, the MIDI/I_2 molar ratio in the new electrolyte was fixed at 20; the electrolyte based on MEIDI was the same as that of MIDI.

Figure 4 shows the current–voltage characteristics for three devices based on different imidazolium electrolytes in

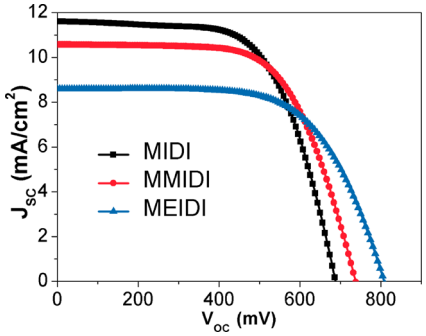

Figure 4. *J-V* characteristics of DSSCs based on MIDI, MMIDI, and MEIDI electrolytes measured under AM1.5 simulated irradiation, 100 mW cm^{-2}.

constituent optimization under 1 sun illumination. At the same experimental conditions, the DSSC employing MIDI gave a short-circuit current density (J_{sc}) of 11.60 mA·cm^{-2}, an open-circuit current density (V_{oc}) of 687 mV, and fill factor (*FF*) of 0.634, leading to a power conversion efficiency (PCE) as high as 5.05 (Table 1). The corresponding values (J_{sc}, V_{oc}, and *FF*)

Table 1. Summary of the Photovoltaic Parameters of DSSCs Based on MIDI, MMIDI, and MEIDI Electrolytes

electrolyte	V_{oc} [mV]	J_{sc} [mA cm^{-2}]	FF	η %
MIDI	687	11.60	63.4	5.05
MMIDI	738	10.58	63.9	4.99
MEIDI	809	8.59	64.0	4.45

of the device based on MMIDI were 10.58 mA·cm^{-2}, 738 mV, and 0.639. The J_{sc}, V_{oc}, and *FF* of a device employing electrolyte based on MEIDI were 8.59 mA·cm^{-2}, 809 mV, and 0.640, respectively. An encouraging 5.05% PCE was achieved based on MIDI. This result indicates that electrolyte based on MIDI is feasible in DSSC with high conversion efficiency. Compared to the properties of DSSCs with MMIDI and MEIDI, the most pronounced change for employing MIDI is the short-circuit current densities (J_{sc}) and open-circuit current density (V_{oc}). The results mean that the J_{sc} and V_{oc} strongly depend on the substituents of the Im^+ cations. Figure 5 shows the influence of

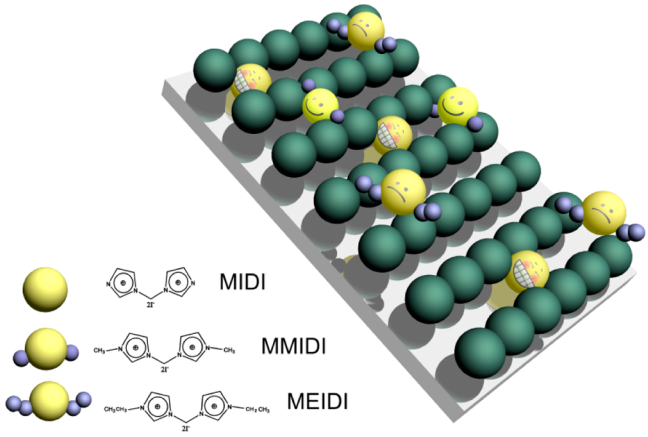

Figure 5. Schematic diagram indicating different bis-Im^+s transferring from electrolyte to photoelectrode. It shows a growing diffusion velocity that the different electrolytes based on MEIDI, MMIDI, and MIDI transfer from electrolyte to photoelectrode in DSSCs.

alkyl chains with diverse Im^+I^-s. From the viewpoint of size of the substituent, this tendency is in agreement with reports that a higher J_{sc} was observed with decreasing alkyl chains, and Im^+ with long alkyl chains enabled an increase in V_{oc}, owing to the increased hydrophobic interactions of the alkyl chains to form barriers for back electron transfer reactions.[22]

To understand the J_{sc} behavior in DSSCs, electrochemical impedance spectroscopy (EIS) was tested. Figure 6a shows the Nyquist plot of the symmetrical Pt–Pt electrochemical cells, and the inset shows the equivalent circuit diagram used to fit the impedance spectrum. The circuit elements consist of charge

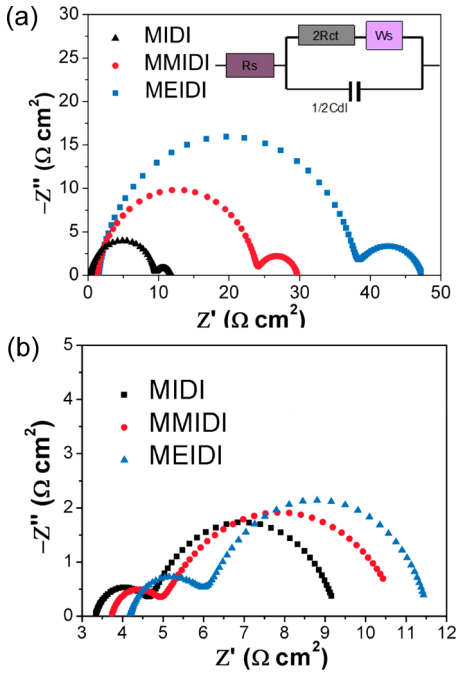

Figure 6. Nyquist plots of DSSC based on MIDI, MMIDI, and MEIDI electrolytes measured (a) on dummy cell and (b) at open circuit condition under AM 1.5, 100 mW cm^{-2} irradiation.

dx.doi.org/10.1021/am400337d | ACS Appl. Mater. Interfaces 2013, 5, 3356–3361

transfer resistance (R_{ct}) at the Pt electrode/electrolyte interface, series resistance (R_s), double layer capacitance (C_{dl}), and Warburg impedance (W_s).[29] The interpretation of such EIS spectrum has been reported elsewhere.[30] The high-frequency semicircle resulted from the charge transfer process at the electrode/electrolyte interface, while the low-frequency arc was attributed to the Nernst diffusion impedance (W_s) of the I^-/I_3^- redox couple in a thin layer of electrolyte.[31,32] The Nyquist plots were fitted and the results are shown in Table 2. The

Table 2. Properties Determined by Electrochemical Impedance Spectroscopy Measurement

electrolyte	R_{ct} [a] [Ω·cm²]	R_k [b] [Ω·cm²]	R_w [b] [Ω·cm²]	ω_k [b] Hz	τ [b] ms	n_s [b] cm⁻³
MIDI	4.5	3.68	2.49	2.60	61.2	10.7×10^{18}
MMIDI	12.0	3.83	2.55	2.20	72.3	12.1×10^{18}
MEIDI	17.8	4.04	6.69	2.05	77.6	12.3×10^{18}

[a]Properties obtained from dummy cells. [b]Properties obtained from DSSCs.

calculated R_{ct} of MIDI-based cell (4.5 Ω·cm²) was smaller than that of MMIDI (12 Ω·cm²) and MEIDI (17.8 Ω·cm²) based cells. This implies that interfacial resistance increased with the DSSC based on larger substituent electrolyte, since the higher interfacial resistance of larger substituent will block the electrons injected from the conductive band of TiO_2 to FTO, the J_{sc} of DSSCs decreased. Figure 6b shows EIS spectrum DSSCs employing MIDI, MMIDI, and MEIDI-based electrolytes measured under 1 sun illumination at open circuit conditions. Table 2 sumarizes the results of EIS analysis calculated by the following equations.

$$\omega_d = \frac{D}{L^2}, \quad \omega_k = k = 1/\tau \tag{1}$$

$$R_w = \mathrm{Con}\frac{L}{D}, \quad R_k = \frac{\omega_d}{\omega_k}R_w = \mathrm{Con}\frac{1}{Lk}, \quad \mathrm{Con} = \frac{k_B T}{q^2 A n_s} \tag{2}$$

Here, R_k, R_w, k_B, τ, T, A, q, and n_s represent charge-transfer resistance related to recombination of an electron, electron transport resistance in TiO_2, Boltzmann constant, lifetime of an electron in TiO_2, absolute temperature, the electrode area, charge of a proton, and the electron density at the steady state in the conduction band, respectively.[33]

$$n_s = N_s e^{(E_F - E_s)/k_B T} \tag{3}$$

$$V_{oc} = -(E_F - E_{F0})/e \tag{4}$$

Here, E_s, N_s, E_F, and E_{F0} reperent lower edge of conduction band, the effective density, the quasi-Fermi level, and the position of the Fermi level in the dark, respectively.[34]

$$\Delta V_{oc} = \frac{k_B T}{e}\ln\frac{n_{s2}}{n_{s1}} = 0.026 \ln\frac{n_{s2}}{n_{s1}} \tag{5}$$

Table 2 shows the n_s of all the samples, the calculated ΔV_{OC} between MEIDI and MMIDI was 0.26 mV (≪ 71 mV), meanwhile the calculated ΔV_{OC} of MMIDI and MIDI was 3.2 mV (≪51 mV), so we can conclude that the trend observed in V_{oc} was not a thermodynamic effect (band displacement). As a consequence, R_w values of DSSC devices based on MIDI, MMIDI, and MEIDI were 2.49, 2.55, and 6.69, respectively. Electron transport resistance of device based on MIDI gained the lowest resistance, which meant it was easy for electron to transport in TiO_2, so the J_{sc} obtained the highest. The charge-transfer resistance related to recombination of electrons of MIDI-based DSSC resulted in the lowest, accompanying with the R_k of device based on MEIDI obtaining the highest, which led to the largest V_{oc} of MEIDI-based device. Through the change of R_k and R_w, the trend observed in V_{oc} was really a kinetic effect.

The electron lifetime in TiO_2 is inversely proportional to the frequency of maximum. As can be seen in Table 2, ω_k values of the devices based on MIDI, MMIDI, and MEIDI were 2.6, 2.2, and 2.05 Hz, respectively, which decreased with larger substituent imidazolium molten salts. Therefore, the electron lifetime (τ) was increased with larger ones.

To understand the origin of the different performance of the devices based on different electrolytes, dark current and open-circuit voltage decay (OCVD) characteristics were measured. Figure 7a shows current−voltage curves in the dark. The dark current is due to recombination at the photoelectrode/electrolyte interface. In this measurement, electrons transport from FTO into photoelectrode and reduce triiodide to iodide, which is opposite in sense to a photocurrent at voltages below V_{oc}. The dark current will increase if it is difficult for electrons transferring from photoelectrode to electrolyte. Otherwise, the dark current will decrease. As expected from the electrochemical studies, it can be seen that the V_{oc} decreases with the increase of dark current. And the dark current of MIDI shows higher than that of MMIDI and MEIDI, which indicates that

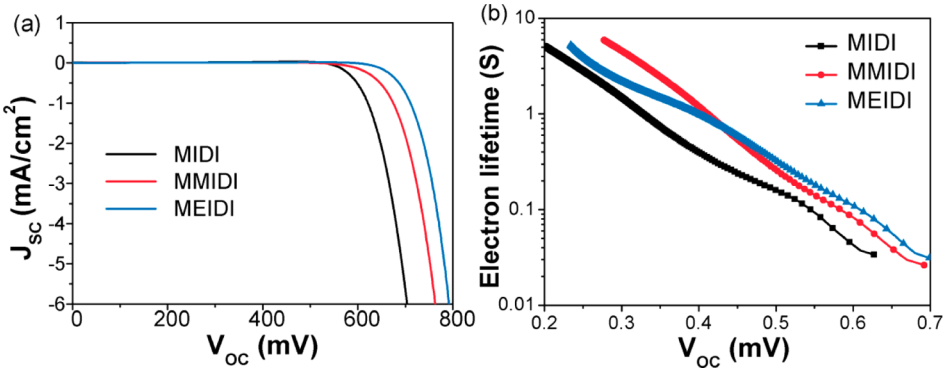

Figure 7. (a) J−V characteristics under dark condition and (b) electron lifetime measured from open circuit voltage decay of DSSCs based on MIDI, MMIDI, and MEIDI electrolytes.

the recombination at the photoelectrode/electrolyte interface of MEID is the lowest, resulting in that the device based on MEIDI obtained the highest voltage of all. OCVD is a technique which monitors the subsequent decay of photovoltage after turning off the illumination in a steady state.[35] The relationship between the electron lifetime and the decay rate is described as[36]

$$\tau = \frac{-k_B T}{e}\left[\frac{dV_{oc}}{dt}\right]^{-1}$$

The increase of V_{oc} in DSSC device based on imidazolium iodide was also attributed to the reduced back recombination at TiO_2/electrolyte interface, and revealed by the longer electron lifetime (Figure 7b) resulting in an improved *FF*. In the measurement of OCVD, during the decay of V_{oc}, electron concentration evolves from the initial steady state value to the dark equilibrium (V_{oc} = 0) with concentration n_0. We will generally neglect the final region of decay at $V_{oc} \approx 50$ mV or less, which is poorly resolved in the current setup, hence we can assume that $n \ll n_0$, while V decreases by about 0.6 V; the value of the curve at high voltage (>0.6 V) mainly reflects the electron lifetime in the photoanode under working conditions.[37] Figure 7b shows that τ_n of the DSSC device based on MMIDI is longer than that of MIDI, and the device based on MEIDI has the longest τ_n of all the devices at $V_{oc} > 0.6$ V. The trend of electron lifetime is consistent with EIS. Both dark current and OCVD explain the variety of V_{oc}. It should be noticed that the increase of V_{oc} associated with the mass of iodide source is in good agreement with the results of other measurements.

CONCLUSIONS

In summary, efficient and readily available low-volatility electrolytes based on MIDI, MMIDI, and MEIDI as iodide sources were synthesized and applied in DSSCs. The impact of imidazolium cations with different substituents (sizes of alkyl chains) on the electrochemical behaviors of the I_3^-/I^- electrolytes were investigated. With larger alkyl chains, electrostatic interactions between solvated Im^+ and charge carriers become stronger, and it is more difficult for imidazolium iodides flowing into photoelectrode, thus decreasing the recombination between the electron on TiO_2 conduction band and the I_3^- in the electrolyte. So the MEIDI with the largest alkyl chains leads to longest electron lifetimes and best V_{oc}, meanwhile the MIDI with the smallest alkyls shows highest J_{sc}. Current results suggest that the bis(imidazolium) molten salts could be promising iodide sources in DSSCs, and better performance is expectable by further efforts on optimizing the composition of the electrolyte. Meanwhile, further research for employing bis(imidazolium) molten salts in quasi-solid state DSSC is underway.

AUTHOR INFORMATION

Corresponding Author

*E-mail: xzzhao@whu.edu.cn (X.Z.), gssyhx@whu.edu.cn (S.G.). Tel: +86-27-8764 2784. Fax: +86-27-6875 2569.

Notes

The authors declare no competing financial interest.

ACKNOWLEDGMENTS

This work is financially supported by the National Basic Research Program of China (2011CB933300), National Science Fund for Talent Training in Basic Science (Grant J1210061), and National Natural Science Foundation of China (Grants 51132001, 51272184)

REFERENCES

(1) Schlapbach, L.; Züttel, A. *Nature* **2001**, *414*, 353−358.
(2) Grätzel, M. *Inorg. Chem.* **2005**, *44*, 6841−6851.
(3) Huang, X.; Han, S.; Huang, W.; Liu, X. *Chem. Soc. Rev.* **2013**, *42*, 173−201.
(4) Chung, I.; Lee, B.; He, J.; Chang, R. P.; Kanatzidis, M. G. *Nature* **2012**, *485*, 486−489.
(5) Chae, J.; Kang, M. *J. Power Sources* **2011**, *196*, 4143−4151.
(6) Zhang, X.; Liu, F.; Huang, Q. L.; Zhou, G.; Wang, Z. S. *J. Phys. Chem. C* **2011**, *115*, 12665−12671.
(7) Sauvage, F.; Decoppet, J. D.; Zhang, M.; Zakeeruddin, S. M.; Comte, P.; Nazeeruddin, M.; Wang, P.; Grätzel, M. *J. Am. Chem. Soc.* **2011**, *133*, 9304−9310.
(8) Weiqing, L.; Dongxing, K.; Molang, C.; Linhua, H.; Songyuan, D. *Prog. Chem.* **2012**, *24*, 722−736.
(9) Cheon, J. Y.; Yu, J.; Jeong, H. Y.; Han, C. H.; Jun, Y.; Joo, S. H. *Chem. Commun.* **2012**, *48*, 8057−8059.
(10) Zhang, C.; Chen, S.; Tian, H.; Huang, Y.; Huo, Z.; Dai, S.; Kong, F.; Sui, Y. *J. Phys. Chem. C* **2011**, *115*, 8653−8657.
(11) Zhang, Q.; Liu, X. *Small* **2012**, *8*, 3711−3713.
(12) Roh, D. K.; Patel, R.; Ahn, S. H.; Kim, D. J.; Kim, J. H. *Nanoscale* **2011**, *3*, 4162.
(13) Chang, Y. H.; Lin, P. Y.; Wu, M. S.; Lin, K. F. *Polymer* **2012**, *53*, 2008−2014.
(14) Boschloo, G.; Hagfeldt, A. *Acc. Chem. Res.* **2009**, *42*, 1819−1826.
(15) Chen, C.; Wang, M.; Li, J.; Pootrakulchote, N.; Alibabaei, L.; Ngoc-Ie, C.; Decoppet, J.; Tsai, J.; Grätzel, C.; Wu, C.; Cao, Y.; Bai, Q.; Yu, Y.; Cheng, S.; Liu, D.; Shi, F.; Gao; Wang, P. *J. Phys. Chem. C* **2009**, *113*, 6290−6297.
(16) Quintana, M.; Marinado, T.; Nonomura, K.; Boschloo, G.; Hagfeldt, A. *J. Photochem. Photobiol., A.* **2009**, *202*, 159−163.
(17) Daeneke, T.; Kwon, T.-H.; Holmes, A. B.; Duffy, N. W.; Bach, U.; Spiccia, L. *Nat. Chem.* **2011**, *3*, 213−217.
(18) Cheng, M.; Yang, X.; Li, S.; Wang, X.; Sun, L. *Energy Environ. Sci.* **2012**, *5*, 6290−6293.
(19) Yanagida, S.; Yu, Y.; Manseki, K. *Acc. Chem. Res.* **2009**, *42*, 1827−1838.
(20) Kuang, D.; Klein, C.; Zhang, Z.; Ito, S.; Moser, J.-E.; Zakeeruddin, S. M.; Grätzel, M. *Small* **2007**, *3*, 2094−2102.
(21) Cao, Y.; Zhang, J.; Bai, Y.; Li, R.; Zakeeruddin, S. M.; Grätzel, M.; Wang, P. *J. Phys. Chem. C* **2008**, *112*, 13775−13781.
(22) Wang, P.; Zakeeruddin, S. M.; Comte, P.; Exnar, I.; Grätzel, M. *J. Am. Chem. Soc.* **2003**, *125*, 1166−1167.
(23) Ogihara, W.; Suzuki, N.; Nakamura, N.; Ohno, H. *Polym. J.* **2006**, *38*, 117−121.
(24) Kanzaki, T.; Nakade, S.; Wada, Y.; Yanagida, S. *Photochem. Photobiol. Sci.* **2006**, *5*, 389−394.
(25) Quezada, C. *J. Org. Chem.* **2003**, *671*, 183−186.
(26) Tai, Q.; Chen, B.; Guo, F.; Xu, S.; Hu, H.; Sebo, B.; Zhao, X. Z. *ACS Nano* **2011**, *5*, 3795.
(27) Imoto, K.; Takahashi, K.; Yamaguchi, T.; Komura, T.; Nakamura, J.; Murata, K. *Sol. Energy Mater. Sol. Cells* **2003**, *79*, 459−469.
(28) Roy-Mayhew, J.; Bozym, D.; Punckt, C.; Aksay, I. H.; Yum; Grätzel, M. *ACS Nano* **2011**, *5*, 165−172.
(29) Lee, W. J.; Ramasamy, E.; Lee, D. Y.; Song, J. S. *ACS Appl. Mater. Inter.* **2009**, *1*, 1145−1149.
(30) Joshi, P.; Zhang, L.; Chen, Q.; Galipeau, D.; Fong, H.; Qiao, Q. *ACS Appl. Mater. Inter.* **2010**, *2*, 3572−3577.
(31) Mei, X.; Cho, S. J.; Fan, B.; Ouyang, J. *Nanotechnology* **2010**, *21*, 395202.
(32) Li, G.; Wang, F.; Jiang, Q.; Gao, X.; Shen, P. *Angew. Chem., Int. Ed.* **2010**, *49*, 3653−3656.

(33) Adachi, M.; Sakamoto, M.; Jiu, J.; Ogata, Y.; Isoda, S. *J. Phys. Chem. B* **2006**, *110*, 13872−13880.
(34) Bisquert, J.; Zaban, A.; Greenshtein, M.; Mora-Seró, I. *J. Am. Chem. Soc.* **2004**, *126*, 13550−13559.
(35) Liu, Y.; Zhai, H.; Guo, F.; Huang, N.; Sun, W.; Bu, C.; Peng, T.; Yuan, J.; Zhao, X. *Nanoscale* **2012**, *4*, 6863−6869.
(36) Zaban, A.; Greenshtein, M.; Bisquert, J. *ChemPhysChem* **2003**, *4*, 859−864.
(37) Kuang, D.; Klein, C.; Ito, S.; Moser, J. E.; Humphry-Baker, R.; Evans, N.; Duriaux, F.; Grätzel, C.; Zakeeruddin, S. M.; Grätzel, M. *Adv. Mater.* **2007**, *19*, 1133−1137.